Preprint: AAS 15-413, AAS/AIAA Space Flight Mechanics Meeting, Williamsburg, VA, Jan, 2015.

AAS 15-413

A LABELED MULTI-BERNOULLI FILTER FOR SPACE OBJECT TRACKING

Brandon A. Jones* **and Ba-Ngu Vo†**

To maintain custody of the increasing number of detectable objects in Earth orbit, tracking systems require robust methods of multi-target state estimation and prediction. One alternative to the classic multiple hypothesis and probabilistic data association methods uses a random finite set for modeling the multi-target state. The common forms of such filters sacrifice knowledge of specific targets for the sake of tractability. This paper presents a labeled multi-Bernoulli filter for tracking space objects, which allows for the identification of individual targets. This version of the filter includes a new-target birth model based on the admissible region and non-Gaussian propagation of the single-target state probability density function. The benefits of the filter are then demonstrated for the tracking of both previously known and newly detected objects near geosynchronous orbit.

INTRODUCTION

One of the principal challenges in space surveillance is the correct association of observations with objects in a given catalog. For observations with an ambiguous or null correlation, difficulty remains in resolving the multiple viable hypotheses, instantiating a new object in the catalog, or accounting for events (e.g., maneuvers) that reduce the association probability. Measurements may be associated with known targets or each other, and the latter case aids in estimating the state of a newly identified object. Several astrodynamics-based methods have been proposed for observation association[1–5] with no single method optimal for all cases. In the event of no viable association hypotheses, an observation is deemed an UnCorrelated Track (UCT). Methods and tools developed for multi-target filtering provide a potential means for preventing or limiting the generation of UCTs by performing data association and state estimation within a single framework. Such filters model processes such as new-target birth and estimate the multi-target state in difficult observation environments (e.g., reduced signal-to-noise ratios). This paper presents the use of a Labeled Multi-Bernoulli (LMB) filter for tracking known and newly discovered space objects while maintaining knowledge of target identification.

Multi-target filters estimate the number of objects in a given surveillance region and their states. Traditional methods such as Multiple Hypothesis Trackers (MHT)[6–8] and Joint Probabilistic Data Association (JPDA)[9] seek to perform such tasks. Alternatively, methods based on Random Finite Sets (RFS) seek the probability density function (PDF) of the multi-target state, which encapsulates uncertainty in the number of objects and the states of the objects as a whole.[10] FInite Set STatistics

*Assistant Research Professor, Department of Aerospace Engineering Science, University of Colorado at Boulder, UCB 431, Boulder, CO, 80309, United States of America, 303-492-3753,Brandon.Jones@colorado.edu

†Professor, Department of Electrical and Computer Engineering, GPO Box U1987, Curtin University, Perth, WA, 6485, Australia, +61-8-9266-3746, ba-ngu.vo@curtin.edu.au

(FISST) provides the mathematical tools for characterizing and analyzing uncertainty in multi-target states, which is consistent with standard probability theory.[11] Central to the RFS multi-target tracking approach is the Bayes multi-target filter that propagates the posterior PDF of the multi-target state forward in time.

Previous applications of RFS-based multi-target filters for tracking orbital debris include the use of the Bernoulli filter–a special case of the Bayes multi-target filter for at most one target,[12–14] the Probability Hypothesis Density (PHD) filter,[15,16] and the Cardinalized Probability Hypothesis Density (CPHD) filter.[16,17] The fundamental forms of these filters maintain no identifying information, e.g., a tail number, which led to the development of tactical importance functions[10] or tagging a given element with an integer identifier.[18] In Reference 19, the notion of labeled RFSs was introduced to address target trajectories and their identities, and an analytic solution to the Bayes multi-target tracking filter known as the generalized labeled multi-Bernoulli (GLMB) filter was derived. An implementation of this filter is detailed in Reference 20. The LMB filter used here is a principled approximation of the GLMB filter, which is capable of tracking a large number of targets. It was demonstrated in Reference 21 that the LMB filter can track up to 1,500 objects using a laptop computer.

This paper presents the use of the LMB filter for tracking multiple space objects in the near-geosynchronous region. The simulated scenario includes both previously known and unknown targets. In the context of multi-target tracking, instantiating a new object in the multi-target state can be treated as *new target birth*. In astrodynamics, this is known as Initial Orbit Determination (IOD). Given the limited information content of a single arc of data, IOD for space debris is non-trivial and a current topic of research.[4,5,22,23] In this paper, the LMB filter is combined with the admissible region approach to modeling birth, which was previously demonstrated with the CPHD filter,[17] and an entropy-based method for orbit state PDF without any assumption on a Gaussian posterior.[24] In addition to modeling new target birth, this paper demonstrates the ability of the LMB filter to maintain identity for previously known targets while updating their state within the prediction and update equations. Additionally, different values for clutter density and detection probability are considered.

The paper is organized as follows. The next section describes the LMB filter as an approximation to the multi-target Bayes filter. This includes a description of random finite sets and their representation as a generalized labeled multi-Bernoulli distribution. The section then presents the details on the LMB filter with a Gaussian mixture approximation. The next section then demonstrates the ability of the LMB to track both known and initially unknown targets while maintaining the correct track label on the previously acquired targets. Finally, conclusions are discussed.

THE LABELED MULTI-BERNOULLI FILTER

This section provides a brief introduction to the general Bayes multi-target filter, random finite sets, and the LMB filter considered in this work. The sections related to the Bayes and LMB filters summarize the presentations provided in References 19, 20 and 25 with some customization for a Gaussian mixture implementation via the Unscented Kalman Filter (UKF).[26] More details on the methods, including derivations where applicable, may be found in those references. The remainder of the section describes augmentations added to the filter for tracking space objects.

Bayes Multi-Target Filtering

In the RFS approach, the multi-target state X_k and observation Y_k at time t_k are represented by the finite sets

$$X_k = \{x_1, x_2, \ldots, x_n\} \subset \mathbb{X} \quad (1)$$

$$Y_k = \{y_1, y_2, \ldots, y_m\} \subset \mathbb{Y} \quad (2)$$

where $\mathbb{X}$ and $\mathbb{Y}$ denote the single-target state and measurement spaces respectively. Note that the $|X_k| = n$ does not necessarily equal $|Y_k| = m$ due to missed detections and clutter. Each single-target state is assumed to be a random vector with realization $x_i \in \mathbb{X}$. Each observation y_j is a vector in $\mathbb{Y}$. Except where required for the sake of clarity, the observation RFS will simply be denoted by Y. The Bayes multi-target filter is an extension of the single-target Bayes filter to propagate the PDF of the multi-target state forward in time.

Like the single-target Bayes filter, the multi-target filter requires the combination of a prediction and measurement update of the multi-target PDF. The predicted multi-target PDF from t_{k-1} to t_k is given by the multi-target Chapman Kolmogorov equation[10]

$$\pi_{k|k-1}\left(X_{k|k-1}\right) = \int f\left(X_{k|k-1}|X\right) \pi(X)\, \delta(X) \quad (3)$$

where $f\left(X_{k|k+1}|X\right)$ is the Markov transition kernel that describes the temporal evolution of the multi-target state, and

$$\int f(X)\, \delta X = \sum_{i=0}^{\infty} \frac{1}{i!} \int f\left(\{x_1, x_2, \ldots, x_i\}\right)\, d\left(x_1, x_2, \ldots, x_i\right) \quad (4)$$

is a set integral. The transition kernel $f\left(X_{k|k-1}|X\right)$ includes the propagation of surviving-target states and accounts for other processes such as new-target birth and spawning. Each existing target has probability $p_s(x)$ of surviving from t_{k-1} to t_k.

Given the predicted PDF $\pi_{k|k-1}$, the posterior multi-target PDF when given the observation Y is given by Bayes rule

$$\pi_k\left(X_k|Y\right) = \frac{g(Y|X_{k|k-1})\pi_{k|k-1}(X_{k|k-1})}{\int g(Y|X)\pi_{k|k-1}(X)\delta X} \quad (5)$$

where $g(Y|X)$ is the multi-target likelihood function that models the output of a given sensor. In this context, $g(Y|X)$ also accounts for clutter measurements and missed detections. The latter property is described by a probability of detection $p_D(x)$. Models for clutter may take one of several forms, with more details on the model employed here to follow.

Notation

The remainder of the LMB filter description follows the notation and abbreviations presented in this section. As implied previously, lower-case letters denote single-target quantities (e.g., x is a single target state) while upper-case letters signify sets (e.g., X is an RFS with elements x_i). As introduced in the following section, some single-target states are augmented with a track identifier. These quantities, sets of these vectors, and PDFs of these sets are denoted by bold-type fonts (e.g., $\boldsymbol{x}$, $\boldsymbol{X}$, and $\boldsymbol{\pi}$). Spaces are indicated by black-board bold letters (e.g., $\mathbb{N}$, $\mathbb{X}$, and $\mathbb{L}$). The function

$\mathcal{F}(\mathbb{X})$ represents the collection of all finite subsets of $\mathbb{X}$ while $\mathcal{F}_n(\mathbb{X})$ instead indicates the collection of all finite subsets with cardinality n.

Some notational abbreviations are also used to simplify the presentation of the multi-target filters in the following sections. The multi-object exponential is

$$[f]^X \equiv \prod_{x \in X} f(x) \tag{6}$$

with $f^{\emptyset} = 1$. The inner product of functions $f(x)$ and $g(x)$ is

$$\langle f(\cdot), g(\cdot) \rangle \equiv \int_{\mathbb{X}} f(x) g(x)\, dx. \tag{7}$$

A generalized delta function, which supports sets, vectors, etc., is defined as

$$\delta_A(B) \equiv \begin{cases} 1 & \text{if } B = A \\ 0 & \text{otherwise.} \end{cases} \tag{8}$$

The inclusion function is given by

$$1_A(B) \equiv \begin{cases} 1 & \text{if } B \subseteq A \\ 0 & \text{otherwise.} \end{cases} \tag{9}$$

For the case where $B = \{b\}$ (i.e., B is a singleton), then $1_A(b)$ may be used instead of the full $1_A(B)$.

Labeled Multi-Bernoulli RFS

The Bernoulli RFS X describing a single target is parameterized by the probability of existence r and the PDF $p(x)$ describing the state $x \in \mathbb{X}$. The probability density function for X is then[10]

$$\pi(X) = \begin{cases} 1 - r & X = \emptyset \\ r \cdot p(x) & X = \{x\}. \end{cases} \tag{10}$$

The multi-Bernoulli RFS $\left\{ \left(r^{(i)}, p^{(i)} \right) \right\}_{i=1}^{M}$ then describes a union of M Bernoulli RFSs each parameterized by $r^{(i)}$ and $p^{(i)}$, which describes a multi-target state. The PDF of $X = \{x_1, x_2, \ldots, x_n\}$ in the multi-target case is then[27]

$$\pi(\{x_1, x_2, \ldots, x_n\}) = \prod_{j=1}^{M} \left(1 - r^{(j)} \right) \sum_{1 \leq i_1 \neq \ldots \neq i_n \leq M} \prod_{l=1}^{n} \frac{r^{(i_l)} p^{(i_l)}(x_l)}{1 - r^{(i_l)}} \tag{11}$$

As described in Reference 19, the multi-Bernoulli RFS may be augmented by a label $\ell = (k, i) \in \mathbb{L}_k$ where k indicates the time of birth (e.g., the subscript in t_k) and $i \in \mathbb{N}$ is a unique index that distinguishes between new targets identified at a common time. The space of labels $\mathbb{L}$ is given by the union of single-time label space $\mathbb{L}_k$, that is $\mathbb{L} \equiv \mathbb{L}_{0:k} = \bigcup_{j=0}^{k} \mathbb{L}_j$. The RFS with track-labeled elements $\boldsymbol{x} = (x, \ell) \in \mathbb{X} \times \mathbb{L}$ is then $\boldsymbol{X} = \{\boldsymbol{x}_1, \ldots, \boldsymbol{x}_n\}$.

Labels ℓ are unique for each possible target, and, to enforce this property, some notation must be defined to properly formulate the labeled multi-Bernoulli density function. The projection $\mathcal{L}(x, \ell) =$

ℓ where $\mathcal{L} : \mathbb{X} \times \mathbb{L} \to \mathbb{L}$ allows for defining the set of RFS labels $\mathcal{L}(\boldsymbol{X}) = \{\mathcal{L}(\boldsymbol{x}) : \boldsymbol{x} \in \boldsymbol{X}\}$. Since each possible target has a unique label, $|\mathcal{L}(\boldsymbol{X})| = |\boldsymbol{X}|$. To simplify notation,

$$\Delta(\boldsymbol{X}) = \delta_{|\boldsymbol{X}|}(|\mathcal{L}(\boldsymbol{X})|) \tag{12}$$

denotes a distinct label indicator.

The labeled multi-Bernoulli RFS is parameterized by $\left\{\left(r^{(\ell)}, p^{(\ell)}\right)\right\}_{\ell\in\mathbb{L}}$, which, to here simplify notation, assumes that the label ℓ may also be used to identify component elements. However, such a simplification is not strictly required.[19] The PDF of $\boldsymbol{X}$ is then

$$\begin{aligned}\boldsymbol{\pi}(\boldsymbol{X}) &= \delta_{|\boldsymbol{X}|}(\mathcal{L}(\boldsymbol{X}))\prod_{i\in\mathbb{L}}\left(1-r^{(i)}\right)\prod_{\ell\in\mathcal{L}(\boldsymbol{X})}\frac{1_{\mathbb{L}}(\ell)r^{(\ell)}}{1-r^{(\ell)}}p^{(\ell)}(x_\ell) &(13)\\ &= \Delta(\boldsymbol{X})w(\mathcal{L}(\boldsymbol{X}))p^{\boldsymbol{X}} &(14)\end{aligned}$$

where

$$\begin{aligned}w(L) &= \prod_{i\in\mathbb{L}}\left(1-r^{(i)}\right)\prod_{\ell\in L}\frac{1_{\mathbb{L}}(\ell)r^{(\ell)}}{1-r^{(\ell)}} &(15)\\ p(x,\ell) &= p^{(\ell)}(x). &(16)\end{aligned}$$

The LBM can be generalized to a mixture of multi-target exponentials, known as a generalized labeled multi-Bernoulli (GLMB)

$$\boldsymbol{\pi}(\boldsymbol{X}) = \Delta(\boldsymbol{X})\sum_{c\in\mathbb{C}}w^{(c)}(\mathcal{L}(\boldsymbol{X}))\left[p^{(c)}\right]^{\boldsymbol{X}} \tag{17}$$

where $\mathbb{C}$ is an index set that can be used for enumerating the set of hypotheses in a multi-target tracking problem, and

$$\begin{aligned}\sum_{L\subseteq\mathbb{L}}\sum_{c\in\mathbb{C}}w^{(c)}(\mathcal{L}(\boldsymbol{X})) &= 1 &(18)\\ \int p^{(c)}(x,\ell)\,dx &= 1. &(19)\end{aligned}$$

The weights $w^{(c)}$ sum to unity over all possible subsets of track labels (accounts for possibility of target existence) and association hypotheses (accounts for distribution in single-target space).

A special form of the GLMB PDF dubbed the δ-GLMB, allows for a more intuitive description of a GLMB in the context of multi-target tracking.[19,20] For the δ-GLMB density, the index set $\mathbb{C}$ is defined over all subsets of $\mathbb{L}$ and a space Ξ representing the history of measurement associations to a given track. Hence,

$$\begin{aligned}\mathbb{C} &= \mathcal{F}(\mathbb{L})\times\Xi &(20)\\ w^{(c)}(L) &= w^{(I,\xi)}\delta_I(L) &(21)\\ p^{(c)} &= p^{(I,\xi)} = p^{(\xi)} &(22)\end{aligned}$$

where $c = (I,\xi)$, $\xi \in \Xi$, and $I \subset \mathbb{L}$. Then, the δ-GLMB density is given by

$$\boldsymbol{\pi}(\boldsymbol{X}) = \Delta(\boldsymbol{X})\sum_{(I,\xi)\in\mathcal{F}(\mathbb{L})\times\Xi}w^{(I,\xi)}\delta_I(\mathcal{L}(\boldsymbol{X}))\left[p^{(\xi)}\right]^{\boldsymbol{X}}. \tag{23}$$

The δ-GLMB is distinguished from the GLMB by the construction of the space $\mathbb{C}$ imposed in its formulation. In the following sections, a hypothesis refers to a single pair (I, ξ) that describes a set of targets by the label set I and measurement association history ξ. The weight $w^{(I,\xi)}$ then describes the probability of hypothesis (I, ξ).

If desired, a cardinality distribution and a PHD may be computed from the δ-GLMB.[19] The cardinality distribution is given by

$$\boldsymbol{\rho}(n) = \sum_{(I,\xi)\in\mathcal{F}_n(\mathbb{L})\times\Xi} w^{(I,\xi)}. \tag{24}$$

The PHD is then found via

$$v(x) = \sum_{\ell\in\mathbb{L}} \sum_{(I,\xi)\in\mathcal{L}(\mathbb{L})\times\Xi} w^{(I,\xi)} 1_I(\ell) p^{(\xi)}(x,\ell). \tag{25}$$

The cardinality distribution and PHD will be used later for track extraction and identification of significant hypotheses for the update step.

The LMB filter employs a closed-form solution for prediction and an approximate update step. The latter step generates an exact update via a δ-GLMB update that is then approximated by an LMB with matching PHD or first moment. The δ-GLMB filter is a closed-form solution to the Bayes multi-target filter, but at the cost of an exponential increase in the number of terms in the prediction step.[19] This is avoided by using the LMB filter. The effects of the transition between the δ-GLMB and LMB PDFs are illustrated in Section III.C of Reference 25. The net effect can include changes in the density of a target ($p^{(\xi)}$) and the weights ($w^{(I,\xi)}$).

LMB Filter: Prediction

The LMB filter uses a closed-form solution to the prediction equation (Eq. 3) for LMB PDFs given in Eq. 14.[25] The prediction step begins with the posterior LMB approximation of the multi-target state parameterized by $\left\{\left(r_{k-1}^{(\ell)}, p_{k-1}^{(\ell)}\right)\right\}_{\ell\in\mathbb{L}}$. Given an LMB form of the birth RFS with density

$$\boldsymbol{\pi}_B(\boldsymbol{X}) = \Delta(\boldsymbol{X}) w_B(\mathcal{L}(\boldsymbol{X})) \left[p_B\right]^{\boldsymbol{X}} \tag{26}$$

and parameter set $\left\{\left(r_B^{(i)}, p_B^{(i)}\right)\right\}_{i=1}^{N_B}$, the prediction presented here accounts for existing target survival and newborn targets. Spawning processes are not included in this description. The weights $w_B(I)$ may be computed via Eq. 15 with existence probabilities $r_B^{(i)}$. The predicted PDF $\boldsymbol{\pi}_{k|k-1}$ is then an LMB with parameter set

$$\left\{\left(r_{k|k-1}^{(\ell)}, p_{k|k-1}^{(\ell)}\right)\right\}_{\ell\in\mathbb{L}} = \left\{\left(r_{S,k|k-1}^{(\ell)}, p_{S,k|k-1}^{(\ell)}\right)\right\}_{\ell\in\mathbb{L}_{0:k-1}} \cup \left\{\left(r_B^{(\ell)}, p_B^{(\ell)}\right)\right\}_{\ell\in\mathbb{L}_k}$$

where $\mathbb{L} = \mathbb{L}_{0:k-1} \cup \mathbb{L}_k$, and

$$r_{S,k|k-1}^{(\ell)} = \eta_S(\ell) r_{k-1}^{(\ell)} \tag{27}$$

$$p_{S,k|k-1}^{(\ell)} = \frac{\left\langle p_s(\cdot,\ell) f(x|\cdot,\ell), p_{k-1}(\cdot,\ell)\right\rangle}{\eta_S(\ell)} \tag{28}$$

$$\eta_S(\ell) = \left\langle p_s(\cdot,\ell), p_{k-1}(\cdot,\ell)\right\rangle. \tag{29}$$

Note the distinction between 's' (in the survival probability $p_s(x,\ell)$) and 'S' (in the PDF of surviving target $p^{(\ell)}_{S,k|k-1}$). This prediction of an LMB with surviving and birth targets is closed under Eq. 3.[25] Eq. 28 indicates that prediction of the surviving-target density $p_S(x,\ell)$ uses a description of the single-target Markov transition density $f(\cdot|\cdot,\ell)$ for target ℓ. The value $\eta_S(\ell)$ is the probability of survival for track ℓ. In the the case of a Gaussian Mixture Model (GMM) implementation

$$p_{k-1}(x,\ell) = 1_{\mathbb{L}}(\ell)\sum_{j=1}^{J}\omega^{(j)}_{k-1}(\ell)\,\mathcal{N}\left(x;\overline{x}^{(j)}_{k-1}(\ell),P^{(j)}_{k-1}(\ell)\right) \tag{30}$$

with state-independent survival probability $p_s(x,\ell) = p_s(\ell)$, then

$$r^{(\ell)}_{S,k|k-1} = p_s(\ell)\,r^{(\ell)}_{k-1} \tag{31}$$

$$p^{(\ell)}_{S,k|k-1} = 1_{\mathbb{L}}(\ell)\sum_{j=1}^{J}\omega^{(j)}_{k|k-1}(\ell)\,\mathcal{N}\left(x;\overline{x}^{(j)}_{k|k-1}(\ell),P^{(j)}_{k|k-1}(\ell)\right) \tag{32}$$

where $\omega_{k|k-1} = \omega_k$ and each Gaussian component with mean $\overline{x}^{(j)}_{k-1}(\ell)$ and covariance $P^{(j)}_{k-1}(\ell)$ is propagated to t_k when using the unscented transformation. As described later, this work instead uses an entropy-based method for approximating the propagated orbit-state PDF. This produces a solution with the same GMM form as Eq. 32, but with possibly more components and different solutions for the weights and Gaussian components. If desired, the$M_{\max}$ elements of the predicted LMB parameter set with the largest existence probabilities $r^{(\ell)}_{k|k-1}$ may be kept, which reduces the complexity of the conversion to a δ-GLMB process described next.

The update step for the LMB filter uses the closed-form δ-GLMB density update presented in Reference 19. Hence, the predicted LMB must then be converted to a δ-GLMB via

$$\boldsymbol{\pi}_{k|k-1}(\boldsymbol{X}_{k|k-1}) = \Delta(\boldsymbol{X}_{k|k-1})\sum_{I\in\mathcal{F}(\mathbb{L})} w^{(I)}_{k|k-1}\delta_I(\mathcal{L}(\boldsymbol{X}_{k|k-1}))\left[p_{k|k-1}\right]^{\boldsymbol{X}_{k|k-1}} \tag{33}$$

with hypothesis weights

$$w^{(I)}_{k|k-1} = \prod_{\ell\in\mathbb{L}}\left(1-r^{(\ell)}_{k|k-1}\right)\prod_{\ell'\in L}\frac{1_{\mathbb{L}}(\ell')r^{(\ell')}_{k|k-1}}{1-r^{(\ell')}_{k|k-1}}. \tag{34}$$

This generates a predicted δ-GLMB used later for the update step in the filter where hypotheses are now based on all possible subsets of the full label space $\mathbb{L}$. All hypotheses use the same spatial density terms $p^{(\ell)}_{k|k-1}$ from the predicted LMB, which consitutes one source of error in using LMB to approximate multi-target PDFs.

The generation of the terms in Eq. 33 may be costly for a large number of tracks. To reduce the computation cost, the K-most significant terms may be computed and used.[19,20,25] In summary, such an algorithm generates the K terms with the largest weights $w^{(I)}_{k|k-1}$ without computing all terms in the series. The maximum number of terms K is then a design parameter for the filter.

LMB Filter: Update

The update step in the filter operates on the predicted δ-GLMB PDF, which is then approximated as an LMB PDF, before track extraction and prediction to the next step.[25] Before performing the update step, some truncations of the hypotheses reduces the computation complexity.

The LMB filter presented in Reference 25 uses spatial groupings of observations and targets to reduce the number of terms in the updated δ-GLMB. While the filter employed for this work does not group targets in the same manner, the set Y is reduced to remove any observation not within some gating distance from the existing and birth tracks. When using an update based on groupings, some alterations of the following methods are required to account for probability of being included in a given group. This presentation does not include these changes, but the addition of such tools in the implementation will likely reduce computation time. Such grouping was used for demonstrating the use of the filter for large-scale multi-target tracking.[21]

Like the prediction step, the measurement update yields an exponential increase in the number of hypotheses to consider. While an enumeration of all possible combinations can be employed, the L most significant hypotheses may instead be used in the update. Murty's algorithm provides one method for identifying the most significant hypotheses to consider.[28] Inputs to the ranked assignment algorithms are based on a CPHD look-ahead. The predicted cardinality distribution and PHD may be computed directly from the δ-GLMB (see Eqs. 24 and 25), which allows for embedding a CPHD measurement update within the LMB filter. Many of the quantities computed in the CPHD may be reused later in the LMB filter update. Details on the procedure for computing the L most significant hypotheses using Murty's algorithm and a CPHD update may be found in Reference 20.

After generating the L most significant hypotheses, the updated LMB density may be generated. As discussed in Reference 25, this update uses the δ-GLMB update proposed in References 19 and 20 with the updated hypothesis weights used to generate the parameters of the LMB process. The update is given by

$$r_k^{(\ell)} = \sum_{(I,\theta)\in\mathcal{F}(\mathbb{L})\times\Theta} 1_I(\ell) w^{(I,\theta)}(Y) \tag{35}$$

$$p_k^{(\ell)}(x) = \frac{1}{r^{(\ell)}} \sum_{(I,\theta)\in\mathcal{F}(\mathbb{L})\times\Theta} 1_I(\ell) w^{(I,\theta)}(Y)\, p^{(\theta)}(x,\ell) \tag{36}$$

where

$$w^{(I,\theta)}(Y) \propto w_{k|k-1}^{(I)} \left[\eta_Y^{(\theta)}\right]^I \tag{37}$$

$$p^{(\theta)}(x,\ell\,|\,Y) = \frac{p_{k|k-1}(x,\ell)\psi_Y(x,\ell;\theta)}{\eta_Y^{(\theta)}(\ell)} \tag{38}$$

$$\eta_Y^{(\theta)}(\ell) = \left\langle p_{k|k-1}(\cdot,\ell), \psi(\cdot,\ell;\theta)\right\rangle \tag{39}$$

$$\psi_Y(x,\ell;\theta) = \begin{cases} \dfrac{p_D(x,\ell)\, g\left(y_{\theta(\ell)}|x,\ell\right)}{\kappa(y_{\theta(\ell)})} & \text{if } \theta(\ell) > 0 \\ 1 - p_D(x,\ell) & \text{if } \theta(\ell) = 0, \end{cases} \tag{40}$$

$p_D(x,\ell)$ is the single-target probability of detection and $\kappa(y)$ is the clutter intensity at point $y \in \mathbb{Y}$. With this update, $\Theta \subset \Xi$ represents the space of single-epoch observation to track associations identified via the L most significant hypotheses, and $\theta \in \Theta$ is a single realization such that $\theta : I \to \{0, 1, 2, \ldots, |Y|\}$ where $\theta(i) = \theta(i') > 0$ implies $i = i'$ and $\theta(i) = 0$ denotes a missed detection.

While Eqs. 38-40 are expressed using general PDFs, the Gaussian mixture approximation is

$$\eta_Y^{(\theta)}(\ell) = \sum_{j=1}^{J} \omega_{k,Y}^{(j,\theta)}(\ell) \tag{41}$$

$$p^{(\theta)}(x,\ell\,|\,Y) = \sum_{j=1}^{J} \frac{\omega_{k,Y}^{(j,\theta)}(\ell)}{\eta_Y^{(\theta)}(\ell)} \mathcal{N}\left(x; x_{k,Y}^{(j,\theta)}(\ell), P_k^{(j,\theta)}(\ell)\right) \tag{42}$$

where

$$\omega_{k,Y}^{(j,\theta)}(\ell) = \omega_{k|k-1}^{(j)}(\ell) \begin{cases} \dfrac{p_D(\ell)\, q_j(y_{\theta(\ell)};\ell)}{\kappa(y_{\theta(\ell)})} & \text{if } \theta(\ell) > 0 \\ 1 - p_D & \text{if } \theta(\ell) = 0 \end{cases} \tag{43}$$

$$q_j(y;\ell) = \mathcal{N}\left(y; h\left(x_{k|k-1}^{(j)}(\ell)\right), P_{yy}^{(j)}(\ell)\right) \tag{44}$$

$$x_{k,Y}^{(j,\theta)}(\ell) = \begin{cases} x_k^{(j)}(y_{\theta(\ell)},\ell) & \text{if } \theta(\ell) > 0 \\ x_{k|k-1}^{(j)}(\ell) & \text{if } \theta(\ell) = 0 \end{cases} \tag{45}$$

$$P_k^{(j,\theta)}(\ell) = \begin{cases} P_k^{(j)}(\ell) & \text{if } \theta(\ell) > 0 \\ P_{k|k-1}^{(j)}(\ell) & \text{if } \theta(\ell) = 0, \end{cases} \tag{46}$$

$h(x)$ is the measurement model, $x_k^{(j)}(y,\ell)$, $P_k^{(j)}(\ell)$, and $P_{yy}^{(j)}(\ell)$ are the component mean, covariance, and prediction residual covariance computed via the UKF update with measurement $y \in Y$, and $p_D(\ell)$ is the state independent probability of detection. Gaussian components of $p^{(\theta)}$ may be merged and truncated to reduce memory and computations.[29] Eqs. 35 and 36 use the updated hypothesis weights $w^{(I,\theta)}$ and densities $p^{(\theta)}(x,\ell\,|Y)$ to generate the LMB parameterization $\left\{\left(r_k^{(\ell)}, p_k^{(\ell)}\right)\right\}_{\ell=1}^{M}$. This effectively removes any knowledge of the observation association space Ξ in the multi-target state PDF for the sake of reduced complexity. However, the θ maps may be stored for later analysis.

Track Extraction

The LMB filter employed in this work leverages the cardinality distribution provided via Eq. 24 in combination with the hypothesis weights $w^{(I,\theta)}$ from Eq. 37 to identify tracks for the estimated RFS $\widehat{\boldsymbol{X}}_k$. Upon computing the cardinality distribution from the hypothesis weights, the maximum a posteriori (MAP) value of $\boldsymbol{\rho}(n)$ provides an estimated number of targets $\widehat{n}$. The hypothesis used to extract the estimated RFS is then

$$(\widehat{I},\widehat{\theta}) = \underset{(I,\theta)\in\mathcal{F}(\mathbb{L})\times\Theta}{\arg\max}\; w^{(I,\theta)}\delta_{\widehat{n}}(|I|), \tag{47}$$

which identifies the most likely hypothesis such that there are $\widehat{n}$ targets. The estimated RFS is then given by

$$\widehat{\boldsymbol{X}} \equiv \left\{(\widehat{x},\ell) : \ell \in \widehat{I}, \widehat{x} = \int x p^{(\theta)}(x,\ell)\, dx\right\} \tag{48}$$

where the states $\widehat{x}$ are the mean of the PDF $p^{(\theta)}$. Alternatively, track extraction may be based on existence probabilities in the LMB parameterization.[25]

Birth Model

The LMB filter requires an LMB birth model parameterized by $\left\{\left(r_B^{(i)}, p_B^{(i)}\right)\right\}_{i=1}^{N_B}$. Reuter, et al.[25] propose a measurement-based model that uses observations at time t_{k-1} to define a birth model at t_k. For such a case, $N_B = |Y_{k-1}|$ and $\left(r_B^{(i)}, p_B^{(i)}\right)$ is determined via the i-th observation y_i. Under the common assumption that a measurement may only be generated by one target, measurements with a high probability of association with a known target have a decreased probability of being from a new object. Hence, $r_B^{(i)}$ is dependent on the association probability

$$r_{A,k-1}(y) = \sum_{(I,\theta)\in\mathcal{F}(\mathbb{L})\times\Theta} w_k^{(I,\theta)} 1_\theta(y) \tag{49}$$

where the A subscript denotes association. In other words, the association probability for observation y is approximated by the sum of the hypothesis weights that use y in the update of a target. If a given measurement was not used in any hypothesis (after any truncation), then $r_{A,k-1}(y) = 0$. The existence probability is then given by

$$r_B^{(i)} = r_{B,k}(y_i) = \min\left(r_{B,\max}, \frac{1 - r_{A,k-1}(y_i)}{\sum_{y'\in Y_{k-1}}(1 - r_{A,k-1}(y'))} \cdot \lambda_B\right) \tag{50}$$

where $r_{B,\max}$ is a maximum allowed new-target probability and λ_B is the mean number of new targets per measurement scan.

Given the nonlinear dynamics of orbit propagation and the sensitivity of a propagated state PDF to errors in the initial condition, some care is required when solving for $p_B^{(i)}$ based on a single measurement. In the context of astrodynamics, new-target birth is analogous to IOD. Estimating an orbit from a single arc of data is not trivial, and is dubbed the "too-short arc" problem. Recent research considers the use of the admissible region to allow for hypothesis-free track correlation[4,22] or generating a probabilistic description of the orbit state.[23] Previously, Jones, et al.[17] demonstrate the use of the latter method to formulate a target birth model in the context of the GM-CPHD filter.[30] The LMB filter birth model discussed here uses a similar method for defining p_B based on the admissible region.

The probabilistic initial orbit state based on the admissible region requires a single observation and a set of constraints to limit the space of possible solutions in directions orthogonal to the measurement. For example, in the case of a measurement y comprised of two angles and their rates, the admissible region in the range ρ and range-rate $\dot{\rho}$ space provides limitations on the solution. Common constraints are based on orbit energy and orbital elements, with analytic solutions for mapping such constraints into the ρ-$\dot{\rho}$ plane.[31] Reference 23 presents a method for approximating the admissible region as a Gaussian mixture based on design parameters σ_ρ and $\sigma_{\dot{\rho}}$ describing the covariance matrix for all components. Smaller values for these σ values improves the accuracy of the approximation at the cost of additional components. Given a measurement y, the initial orbit state is

$$p_{B,k-1}^{(i)}(x) = \sum_{j=1}^{J_B} \omega_B^{(j)} \mathcal{N}\left(h(x); \begin{bmatrix} y_i \\ \overline{\rho}^{(j)} \\ \overline{\dot{\rho}}^{(j)} \end{bmatrix}, \begin{bmatrix} R_i & 0 & 0 \\ 0 & \sigma_\rho^2 & 0 \\ 0 & 0 & \sigma_{\dot{\rho}}^2 \end{bmatrix}\right) \tag{51}$$

where J_B is the number of components in the mixture, $\omega_B^{(i)}$, $\overline{\rho}$, and $\overline{\dot{\rho}}$ are the mixture weights and mean in the ρ-$\dot{\rho}$ space, and R_i is the covariance matrix for y_i. If desired, then each component in the

mixture may be converted to Cartesian coordinates using the unscented transformation. The PDF $p^{(i)}_{B,k-1}$ is then propagated to t_k to obtain the density $p^{(i)}_B$ used in the birth model. To better account for the nonlinearity of orbital dynamics, this propagation employs the PDF propagation method described in the next section.

Non-Gaussian PDF Propagation

Orbit state PDF propagation fails to remain Gaussian over sufficiently long durations.[32] The previous description of the LMB filter assumes a GMM representation for the single-target state PDF given by Eq. 32. To compensate for the non-linear orbit state propagation, this work uses an entropy-based method of identifying when to split Gaussian components during propagation. The resulting GMM yields a more accurate approximation of the predicted orbit state PDF. This method, dubbed Adaptive Entropy-based Gaussian Information Synthesis (AEGIS) uses the entropy-based metric to identify when a nonlinear propagation of a Gaussian PDF via the unscented transform deviates from a linear approximation.[24] The instantaneous entropy for the nonlinear solution propagated via the unscented transformation is given by

$$H_{\text{non}} = \frac{1}{2}\log|2\pi eP| \tag{52}$$

while the differential equation for the linear solution is

$$\dot{H}_{\text{lin}}(x) = \text{trace}\left(\frac{\partial F(x,t)}{\partial x}\right) \tag{53}$$

where F is the dynamics model and the linear solution is computed using the mean trajectory. When $|H_{\text{non}} - H_{\text{lin}}| > \tau$ where τ is a given threshold, the two solutions have deviated beyond the approximation accuracy requirement. When this occurs, a given mixture element is split into a predetermined number of components along the covariance matrix principal axis direction corresponding to the largest eigenvalue. Using this method, the number of components may increase with the LMB prediction, but the result remains a GMM. Full details on AEGIS may be found in Reference 24. The implementation used here uses $\tau = 0.003H_0$ where H_0 is computed via Eq. 52 and the initial covariance matrix P.

Clutter Model

A given sensor may produce false measurements, dubbed clutter, which adds complication to the multi-target tracking problem. This work assumes a Poisson distribution for the number of clutter observations in a given scan with a mean of λ_c returns. The LMB filter also requires a description of the clutter intensity $\kappa(y)$ in the measurement space. The measurements are here uniformly distributed in the sensor field of view. Hence,

$$\kappa(y) = \lambda_c \cdot \mathcal{U}(y) \tag{54}$$

where $\mathcal{U}$ denotes a uniform distribution over the field of view.

SIMULATION RESULTS

The performance of the LMB filter for tracking orbital debris is presented in this section. The following sections first provide an overview of the scenario, followed by a presentation of performance for a single execution of the filter, and finally a MC-based test. Both cases consider variations in the mean number of clutter returns and the probability of detection.

Table 1: Initial Conditions for Simulated Spacecraft

Parameter	Target 1	Target 2
Semimajor Axis (km)	42164.573	41169.822
Eccentricity	0.0002878	0.00021
Inclination (deg)	0.006	1.303
Right Asc. of Node (deg)	278.657	189.101
Arg. of Perigee (deg)	139.8697	9.869
True Anomaly (deg)	91.432	-51.024

Test Case Description

All tests of the LMB filter for tracking orbital debris use the same scenario based on tracking space objects in near-geosynchronous orbit via optical measurements. The scenario includes seven targets with two known a priori and the remaining five added to the multi-target state via the previously described birth model. The true initial condition for the known targets is provided in Table 1. The initial state for the remaining five targets is generated by randomly perturbing that of the first target. These random perturbations are Gaussian with zero mean and standard deviations in semimajor axis, inclination, and true anomaly of 200 km, 0.001 deg, and 0.25 deg, respectively. Four of the unknown targets appear at the initial time with the final unknown target appearing with the third measurement scan.

The single-target state estimated by the filter is the inertial position and velocity vector

$$x = \begin{bmatrix} X & Y & Z & \dot{X} & \dot{Y} & \dot{Z} \end{bmatrix}^T. \tag{55}$$

The initial multi-Bernoulli RFS (with $M = 2$) assumes $r^{(i)} = 0.95$ and $p^{(i)}$ is Gaussian. The initial covariance is

$$P = \text{diag}\begin{bmatrix} 1 & 1 & 0.01 & 10^{-6} & 10^{-6} & 10^{-8} \end{bmatrix} \tag{56}$$

with distance and time units in km and sec, respectively. The mean used by the filter is generated by randomly perturbing the true initial condition given P.

The multi-Bernoulli RFSs for the new targets use the birth model described previously. Admissible region constraints are based on semimajor axis and eccentricity. The birth model assumes a maximum eccentricity of 0.1 and a near-geosynchronous orbit semimajor axis range of 42,164.573$\pm$1,400 km. The Gaussian mixture parameters are $\sigma_\rho = 50$ km and $\sigma_{\dot{\rho}} = 0.3$ km/s. The maximum birth target existence $r_{B,\max} = 0.01$ with $\lambda_B = 0.1$ targets per measurement scan define statistics on the birth rate. Increasing both will yield a faster confirmation of a given target at the cost of more clutter tracks.

Table 2 describes the force models for the truth and filter. The filter dynamic model uses a slightly reduced fidelity when compared to the modeled truth. Orbit propagation uses the CU-TurboProp orbit propagation package[37] with the Dormand-Prince 8(7) Runge-Kutta method and a relative tolerance of 10^{-12}. Each Gaussian component in the filter is propagated using the unscented transformation[26] and a linear process noise matrix

$$Q_k = \sigma_Q^2 \cdot \Gamma(t_k, t_{k-1})\Gamma^T(t_k, t_{k-1}) \tag{57}$$

$$\Gamma(t_k, t_{k-1}) = \begin{bmatrix} \dfrac{(t_k - t_{k-1})^2}{2}\mathbb{I}_3 & (t_k - t_{k-1})\,\mathbb{I}_3 \end{bmatrix}^T \tag{58}$$

Table 2: Propagation Model for Measurement Generation and the Filter Dynamics Model

Parameter	Truth Model	Filter Model
Gravity Perturbation Model	GGM03C[33]	GGM02C[34]
Spherical Harmonic Degree/Order	8×8	4×4
Third Bodies	Sun and Moon	Sun and Moon
Planetary Ephemeris	DE430[35]	DE405[36]
Epoch Time (Julian Date)	245611.5	245611.5
Solar Radiation Pressure	On	Off
Coefficient of Reflectivity	1.5	N/A
Area-to-Mass Ratio (m^2/kg)	0.01	N/A
Process Noise σ_Q (km/s^2)	N/A	10^{-11}

where $\mathbb{I}_3$ is a 3×3 identity matrix and $\sigma_Q = 10^{-10}$ km/sec^2. The probability of target survival is $p_s = 0.99$ and no targets leave the sensor field of view.

The elements of the measurement set Y are single-target observations $y \in \mathbb{R}^4$. Each y includes topocentric right ascension, declination, and their rates, and is generated using the true propagated position and velocity. Measurement errors are based on a zero-mean Gaussian distribution with standard deviations of 0.4 arcsec and 0.07 arcsec/s for the angles and angle-rates, respectively, and match those used in Reference 23. The observation-error covariance matrix $R \in \mathbb{R}^{4\times4}$ is based on these values. These simulated measurements are generated via a ground station at

$$r_{\text{sensor}} = \begin{bmatrix} -1519.509 & -5077.663 & 3550.820 \end{bmatrix}^T \text{ km} \tag{59}$$

in the Earth-fixed frame with zero location error. This matches the approximate location of the Ground-based Electro-Optical Deep Space Surveillance (GEODSS) telescope in Socorro, NM.[38] A single scan generates m measurements, which are here affected by the probability of detection and clutter rates. Missed detections are modeled using the designated value of p_D while the number of clutter returns is based on a Poisson distribution with a mean λ_c. The following tests consider two combinations of these values: (i) $p_D = 0.9$ and $\lambda_c = 10$, and (ii) $p_D = 0.75$ and $\lambda_c = 5$. The simulated time period covers a seven-hour window with observations provided at the start, end, and 18 randomly selected times in the interval. This yields a total of 20 measurement scans. The minimum time between observations is five minutes. Clutter measurements are uniformly distributed over the sensor volume. The sensor field of view (FOV) is approximately 2.4×4.4 deg and centered on target 1. For the purposes of generating clutter measurements, the range of angle-rates possible is $\pm10^{-3}$ deg/sec.

Figure 1 illustrates the location of the seven targets in the FOV over the seven-hour simulation time. Since the FOV is centered on target 1, it remains fixed at the center of the figure. For the purposes of visualization for Figure 1, all other tracks are represented as a difference in right ascension and declination with respect to target 1. The figure also provides an example distribution of all observations over the seven hours simulation with a clutter rate of $\lambda_c = 10$ and $p_D = 0.9$. Except for target 2, all objects remain close to each other in the observation space, promoting ambiguity in measurement association for sufficiently diffuse $p^{(\ell)}_{k|k-1}(x)$. Target 2 crosses the path of the other objects at approximately 2.8 hours past the epoch time.

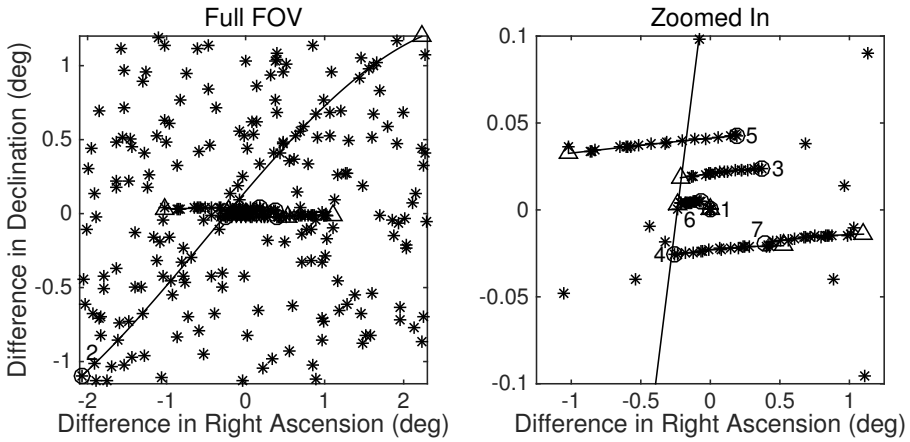

Figure 1: Observations Over All Times and Object Tracks with Start (○) and End (△) Points

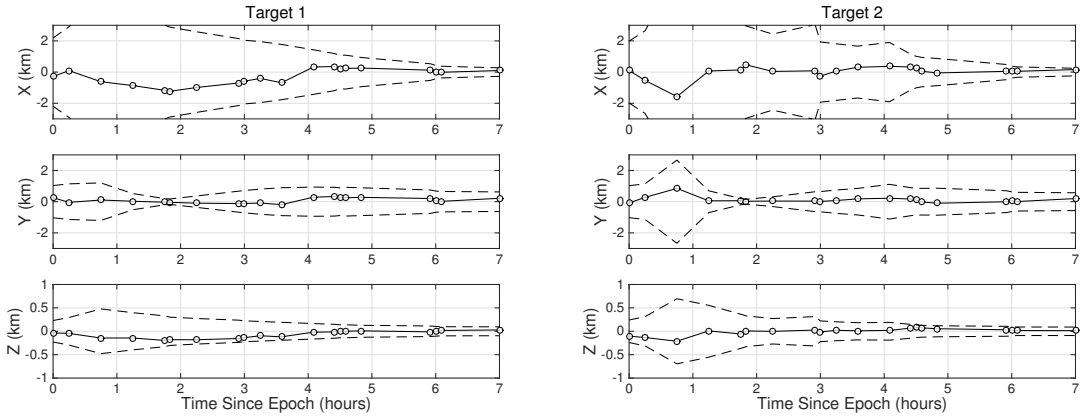

Figure 2: Position Error and 3σ Bounds for Known Targets with $p_D = 0.9$

Single Case

This section presents the performance of the LMB filter with a focus on a single run for each of the λ_c and p_D pairs selected for evaluation. This includes a description of state accuracy for the initially known targets and the multi-target state as a whole. The estimated state error over time is described for the known targets individually as reported by the LMB filter based on the target label ℓ. The full filter accuracy, which includes both the initially known and unknown targets, is presented as an Optimal Sub-Pattern Assignment (OSPA) value, which generalizes the single-target miss distance to a multi-target state.[39] All OSPA values presented in this paper assume a p-norm of 2, a cutoff value (c) of 50 km, and ignore the cardinality penalty term.

Figure 2 presents the state estimation error for the initially known targets with $p_D = 0.9$ and $\lambda_c = 10$. For this case, the filter included these targets as part of the most likely hypothesis $(\widehat{I}, \widehat{\theta})$ at all times in spite of any missed detections. Estimation error converges to less than 1 km in each component direction by the end of the scenario. The errors are also bound by the 3σ boundaries

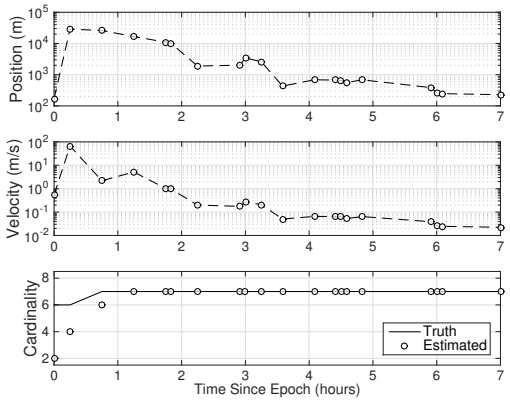

Figure 3: LMB Filter Performance Based on OSPA and Cardinality with $p_D = 0.9$

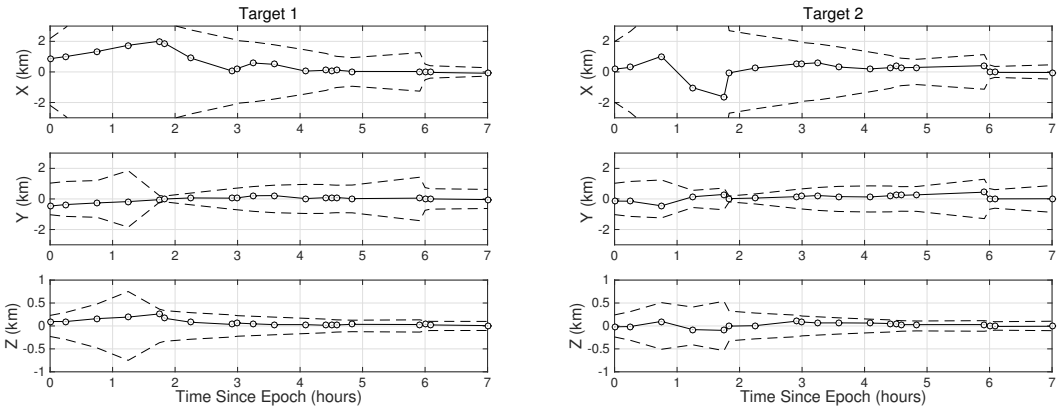

Figure 4: Position Error and 3σ Bounds for Known Targets with $p_D = 0.75$

at all times. The reduced uncertainty in the Y component at approximately 2 hours results from observation geometry.

Performance based on the full multi-target state is illustrated in Figure 3. Early times exhibit a large error due to a non-converged solution for the new targets. In these cases, the error is primarily determined by the cutoff c used in the OSPA calculation. The accuracy results for the known targets confirm that the OSPA error results from the newborn targets. Tighter constraints on the admissible region will reduce the variance on the initial state and improve convergence, but at the potential expense of ignoring the true ρ-$\dot{\rho}$ state. Estimation error in both position and velocity decreases with follow-up observations, which yields final OSPA errors of approximately 228 m and 0.024 m/sec in position and velocity, respectively. The error in the estimated cardinality demonstrates a lag in confirming the presence of the new targets. Since the birth model uses measurements at the previous time for its definition of $p_B^{(i)}$, there will be at least a one-measurement lag in confirming a new target.

Figure 4 illustrates the single-target accuracy for the initially known targets with $p_D = 0.75$ and $\lambda_c = 5$. When compared to the case with a higher p_D, the larger 3σ bounds at the final time

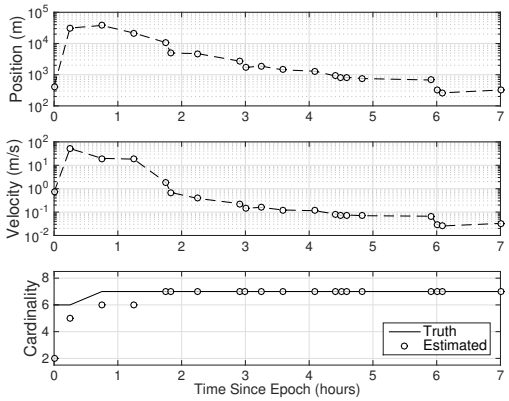

Figure 5: LMB Filter Performance Based on OSPA and Cardinality with $p_D = 0.75$

demonstrate the reduced solution confidence as a result of missed detections. Like the previous case, the filter includes these targets in $\widehat{\boldsymbol{X}}$ at all measurement times. Estimated state accuracy is similar to the case with a higher p_D, although the result for the second known target exhibits larger discrepancies (e.g., due to a missed detection at 1.75 hours).

Figure 5 demonstrates the performance of the LMB filter when considering the full multi-target state with the reduced p_D and λ_c. Due to missed detections, the filter yields a slightly larger OSPA position and velocity error of 323 m and 0.033 m/sec, respectively, at the final time.

Monte Carlo Tests

This section describes the performance of the LMB filter based on a Monte Carlo analysis. The cases described in the previous section are repeated 100 times with different random number generator states. This allows for variations in the number and time of any missed detections, the number of clutter measurements and their values, the initial state of the known targets, and the realized measurement errors. Observation times are fixed for all runs. This analysis is then conducted on both of the p_D-λ_C combinations discussed previously. This presentation does not include any assessment of the accuracy for the initially known targets.

Figure 6 illustrates the distribution of cardinality estimates for the LMB filter with $\lambda_c = 10$ and

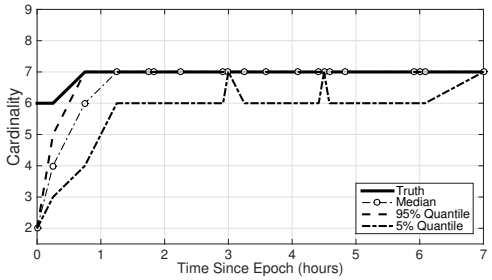

Figure 6: Estimated Cardinality for the $\lambda_c = 10$ and $p_D = 0.9$ Case Over 100 MC Runs

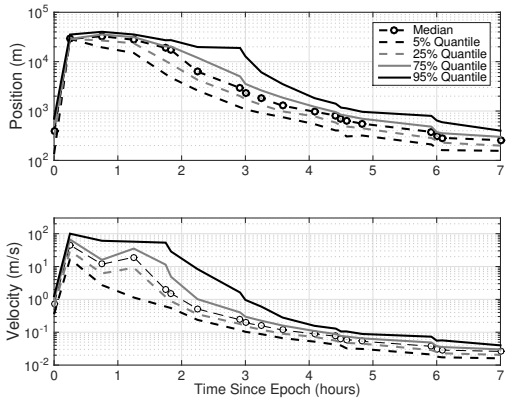

Figure 7: OSPA Distances for the $\lambda_c = 10$ and $p_D = 0.9$ Case Over 100 MC Runs

$p_D = 0.9$. The median cardinality exhibits a lag in the identification of new targets in the multi-target state. Contrary to the previous results, the 95% quantile indicates that some cases identify the presence of seven targets immediately when all are visible. As discussed previously, the adaptive measurement model includes a one-observation lag. Hence, the cases with faster identification of new targets match the true cardinality as a result of clutter tracks. After four observations, the median cardinality and the 95% quantile equal the true value. The number of clutter tracks are reduced at later times due to filter convergence and the one-measurement delay for birth. As the uncertainty on the state of a given target decreases, the hypothesis weight that includes that target also increases. Hence, $r_B^{(i)}$ for observations assigned to an existing target decreases and the case of a new object is rejected by the LMB filter. Clutter measurements typically do not yield clutter tracks for the case presented here because follow-up observations do not confirm their existence. The 5% quantile indicates that the filter multi-target state estimate sometimes fails to report tracks. This is a result of consecutive missed detections for a single target, which reduces its probability of existence.

Figure 7 describes the OSPA position and velocity accuracy for the filter using $\lambda_c = 10$, $p_D = 0.9$, and the 100 MC runs. The position and velocity OSPA results indicate that 95% of the cases converge on a solution with an OSPA accuracy below 400 m and 0.04 m/sec in position and velocity, respectively. Although not depicted, the worst-case OSPA position accuracy is approximately 10.98 km due to the filter losing custody of one of the newborn tracks at 4.58 hours. Hence, the birth model instantiates a new target, which increases the filter error until the solution converges.

The MC results for the $\lambda_c = 5$ and $p_D = 0.75$ case are provided in Figures 8 and 9. Results for the cardinality statistics in Figure 8 differ slightly from those with a higher p_D. The smaller p_D yields an increased delay in confirming the presence of new targets and more clutter tracks. For the previous $p_D = 0.9$ case, the filter produces clutter tracks until the $p^{(i)}$ values for the targets become more concise. For a smaller p_D, the reduced observation density and rate of increase in $\omega_{k,Y}^{(i,\theta)}(\ell)$ (see Eq. 43) causes a delay in convergence. Hence, the period for potential clutter tracks increases. Although the results indicate that the lower p_D yields a more accurate cardinality estimate at later times, this is primarily a result of statistical variation. OSPA results also indicate a slight reduction in filter accuracy, but this is expected given the reduced number of observations per object. However,

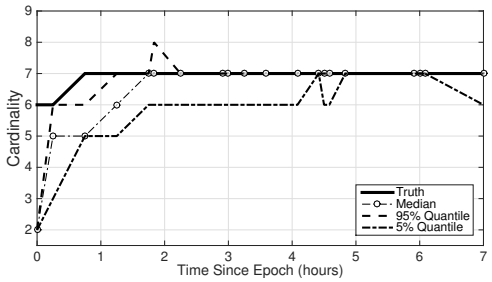

Figure 8: Estimated Cardinality for the $\lambda_c = 5$ and $p_D = 0.75$ Case Over 100 MC Runs

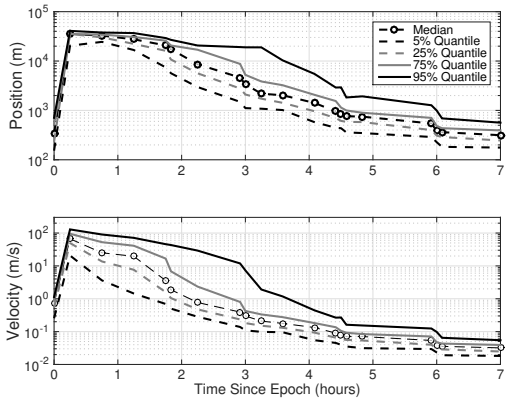

Figure 9: OSPA Distances for the $\lambda_c = 5$ and $p_D = 0.75$ Case Over 100 MC Runs

results indicate the same general trend of convergence to a solution with position and velocity OSPA errors smaller than 600 m and 0.06 m/s, respectively.

CONCLUSIONS

The LMB filter provides a means for tracking multiple space objects while maintaining target identity without the need for a separate track initiation module. The filter uses a labeled multi-Bernoulli RFS with an approximate Bayesian update step for multi-target filtering. Using a birth model based on the admissible region allows for instantiation of new targets in the multi-target state. The propagation of the single-target Gaussian mixture in the prediction step employs an entropy-based method to better approximate the posterior solution. Within the context of the LMB filter, subsequent observation scans allow for maintaining custody and identity of previously known targets while resolving the orbit for newly discovered objects. Filter performance varies with the probability of target detection and the density of clutter measurements, but converges on a solution accurate to less than 1 km in position.

ACKNOWLEDGMENTS

The authors thank Dr. Ba-Tuong Vo of Curtin University for his discussion on the methods employed in the paper.

REFERENCES

[1] P. W. Schumacher, Jr., C. Sabol, A. Segerman, A. Hoskins, S. Coffey, K. Borelli, J. Addison, K. Hill, K. Roe, and B. Duncam, "Search and Determine Integrated Environment (SADIE) for Automated Processing of Space Surveillance Observations," *AIAA/AAS Astrodynamics Conference*, AIAA 2014-4165, San Diego, California, August 4-7 2014, 10.2514/6.2014-4165.

[2] P. W. Schumacher, Jr., "Tracking Satellite Break-Ups," *Proceedings of the 2nd U.S.-Russian Space Surveillance Workshop Conference Proceedings*, 1996, pp. 174–182.

[3] S. L. Coffey, H. L. Neal, and M. M. Berry, "Uncorrelated Observations Processing at Naval Space Command," *Journal of Guidance, Control, and Dynamics*, Vol. 25, 2015/01/03 2002, pp. 676–684, 10.2514/2.4962.

[4] K. Fujimoto, D. J. Scheeres, J. Herzog, and T. Schildknecht, "Association of optical tracklets from a geosynchronous belt survey via the direct Bayesian admissible region approach," *Advances in Space Research*, Vol. 53, No. 2, 2014, pp. 295–308.

[5] M. J. Holzinger, K. K. Luu, C. Sabol, and K. Hill, "Probabilistic Tracklet Characterization and Prioritization Using Admissible Regions," *Proceedings of the 2014 Advanced Maui Optical and Space Surveillance Technologies Conference*, Wailea, Maui, Hawaii, September 9-12 2014.

[6] D. B. Reid, "An Algorithm for Tracking Multiple Targets," *IEEE Transactions on Automatic Control*, Vol. AC-24, December 1979, pp. 843–854.

[7] T. Kurien, *Multitarget-Multisensor Tracking: Advanced Applications*, ch. Issues in the design of practical multarget tracking algorithms. Artech House, 1990.

[8] S. Blackman and R. Popoli, *Design and Analysis of Modern Tracking Systems*. Norwood, MA: Artech House, 1999.

[9] T. E. Fortmann, Y. Bar-Shalom, and M. Scheffe, "Sonar Tracking of Multiple Targets Using Joint Probabilistic Data Association," *IEEE Journal of Oceanic Engineering*, Vol. OE-8, July 1983, pp. 173–184.

[10] R. P. S. Mahler, *Statistical Multisource-Multitarget Information Fusion*. Boston, Massachusetts: Artech House, 2007.

[11] B.-N. Vo, S. Singh, and A. Doucet, "Sequential Monte Carlo methods for multitarget filtering with random finite sets," *Aerospace and Electronic Systems, IEEE Transactions on*, Vol. 41, Oct 2005, pp. 1224–1245, 10.1109/TAES.2005.1561884.

[12] I. I. Hussein, K. J. DeMars, C. Früh, R. S. Erwin, and M. K. Jah, "An AEGIS-FISST Integrated Detection and Tracking Approach to Space Situational Awareness," *2012 15th International Conference on Information Fusion*, Singapore, July 9-12 2012, pp. 2065–2072.

[13] I. I. Hussein, K. J. DeMars, C. Früh, M. K. Jah, and R. S. Erwin, "An AEGIS-FISST Algorithm for Multiple Object Tracking in Space Situational Awareness," *AIAA/AAS Astrodynamics Specialist Conference*, Minneapolis, Minnesota, August 13-16 2012.

[14] I. I. Hussein, C. Früh, R. S. Erwin, and M. K. Jah, "An AEGIS-FISST Algorithm for Joint Detection, Classification and Tracking," *AAS/AIAA Space Flight Mechanics Meeting*, Kauai, Hawaii, February 10-14 2013.

[15] Y. Cheng, K. J. DeMars, C. Früh, and M. K. Jah, "Gaussian Mixture PHD Filter for Space Object Tracking," *AAS/AIAA Space Flight Mechanics Meeting*, Kauai, Hawaii, February 10-14 2013.

[16] S. Gehly, B. A. Jones, and P. Axelrad, "Comparison of Multitarget Filtering Methods as Applied to Space Situational Awareness," *AAS/AIAA Astrodynamics Specialist Conference*, AAS 13-765, Hilton Head, SC, August 11-15 2013.

[17] B. A. Jones, S. Gehly, and P. Axelrad, "Measurement-based Birth Model for a Space Object Cardinalized Probability Hypothesis Density Filter," *AIAA/AAS Astrodynamics Conference*, AIAA 2014-4311, San Diego, California, August 4-7 2014.

[18] K. Panta, D. E. Clark, and B.-N. Vo, "Data Association and Track Management for the Gaussian Mixture Probability Hypothesis Density Filter," *IEEE Transactions on Aerospace and Electronic Systems*, Vol. 45, July 2009, pp. 1003–1016, 10.1109/TAES.2009.5259179.

[19] B.-T. Vo and B.-N. Vo, "Labeled Random Finite Sets and Multi-Object Conjugate Priors," *IEEE Transactions on Signal Processing*, Vol. 61, July 2013, pp. 3460–3475, 10.1109/TSP.2013.2259822.

[20] B.-N. Vo, B.-T. Vo, and D. Phung, "Labeled Random Finite Sets and the Bayes Multi-Target Tracking Filter," arXiv: 1312.2372v1, 2013.

[21] B.-N. Vo, B.-T. Vo, S. Reuter, Q. Lam, and K. Dietmayer, "Towards Large Scale Multi-Target Tracking," *Proceedings of the SPIE, Sensors and Systems for Space Applications VII*, 2014, p. 90850W, 10.1117/12.2055002.

[22] K. Fujimoto and D. J. Scheeres, "Correlation of Optical Observations of Earth-Orbiting Objects and Initial Orbit Determination," *Journal of Guidance, Control, and Dynamics*, Vol. 35, No. 1, 2012, pp. 208–221.

[23] K. J. DeMars and M. K. Jah, "Probabilistic Initial Orbit Determination Using Gaussian Mixture Models," *Journal of Guidance, Control, and Dynamics*, Vol. 36, September - October 2013, pp. 1324–1335.

[24] K. J. DeMars, R. H. Bishop, and M. K. Jah, "Entropy-Based Approach for Uncertainty Propagation of Nonlinear Dynamical Systems," *Journal of Guidance, Control, and Dynamics*, Vol. 36, July-August 2013, pp. 1047–1057.

[25] S. Reuter, B.-T. Vo, B.-N. Vo, and K. Dietmayer, "The Labeled Multi-Bernoulli Filter," *IEEE Transactions on Signal Processing*, Vol. 62, June 2014, pp. 3246–3260, 10.1109/TSP.2014.2323064.

[26] S. J. Julier and J. K. Uhlmann, "Unscented Filtering and Nonlinear Estimation," *Proceedings of the IEEE*, Vol. 92, March 2004, pp. 401–422.

[27] R. P. S. Mahler, *Advances in Statistical Multisource-Multitarget Information Fusion*. Boston, Massachusetts: Artech House, 2014.

[28] K. G. Murty, "An Algorithm for Ranking all the Assignments in Order of Increasing Cost," *Operations Research*, Vol. 16, No. 3, 1968, pp. 682–687, 10.1287/opre.16.3.682.

[29] B.-N. Vo and W.-K. Ma, "The Gaussian Mixture Probability Hypothesis Density Filter," *IEEE Transactions on Signal Processing*, Vol. 54, November 2006, pp. 4091–4104.

[30] B.-T. Vo, B.-N. Vo, and A. Cantoni, "Analytic Implementations of the Cardinalized Probability Hypothesis Density Filter," *IEEE Transactions on Signal Processing*, Vol. 55, July 2007, pp. 3553–3567.

[31] G. Tommei, A. Milani, and A. Rossi, "Orbit determination of space debris: admissible regions," *Celestial Mechanics and Dynamical Astronomy*, Vol. 97, No. 4, 2007, pp. 289–304.

[32] J. L. Junkins, M. R. Akella, and K. T. Alfriend, "Non-Gaussian Error Propagation in Orbital Mechanics," *Journal of the Astronautical Sciences*, Vol. 44, October - December 1996, pp. 541–563.

[33] B. D. Tapley, J. C. Ries, S. V. Bettadpur, D. Chambers, M. Cheng, F. Condi, and S. Poole, "The GGM03 Mean Earth Gravity Model from GRACE," *American Geophysical Union, Fall Meeting*, Abstract No. G42A-03, 2007.

[34] B. Tapley, J. Ries, S. Bettadpur, D. Chambers, M. Cheng, F. Condi, B. Gunter, Z. Kang, P. Nagel, R. Pastor, T. Pekker, S. Poole, and F. Wang, "GGM02 - An Improved Earth Gravity Field Model from GRACE," *Journal of Geodesy*, Vol. 79, No. 8, 2005, pp. 467–478.

[35] W. M. Folkner, J. G. Williams, D. H. Boggs, R. S. Park, and P. Kuchynka, "The Planetary and Lunar Ephemerides DE430 DE431," IPN Progress Report 42-196, Jet Propulsion Laboratory, California Institute of Technology, http://ipnpr.jpl.nasa.gov/progress_report/42-196/196C.pdf, February 2009.

[36] E. M. Standish, "JPL Planetary and Lunar Ephemerides, DE405/LE405," interoffice memorandum IOM 312F-98-048, Jet Propulsion Laboratory, August 26 1998.

[37] K. Hill and B. A. Jones, *TurboProp Version 4.0*. Colorado Center for Astrodynamics Research, May 2009.

[38] D. A. Vallado and W. D. McClain, *Fundamentals of Astrodynamics and Applications*. Hawthorne, CA and New York, NY: Microcosm Press and Springer, third ed., 2007.

[39] D. Shuhmacher, B.-T. Vo, and B.-N. Vo, "A Consistent Metric for Performance Evaluation of Multi-Object Filters," *IEEE Transactions on Signal Processing*, Vol. 56, August 2008, pp. 3447–3457, 10.1109/TSP.2008.920469.